BRAIN SURFACE SEGMENTATION OF MAGNETIC RESONANCE IMAGES OF THE FETUS

D. Ferrario[1], *M. Bach Cuadra*[1], *M. Schaer*[1,2], *N. Houhou*[1], *D. Zosso*[1], *S. Eliez*[2], *L. Guibaud*[3] *and J.-Ph. Thiran*[1]

[1]Signal Processing Laboratories (LTS5), http://lts5www.epfl.ch/
Ecole Polytechnique Fédérale de Lausanne (EPFL), CH-1015 Lausanne, Switzerland
Email: {damien.ferrario,nawal.houhou,dominique.zosso,meritxell.bach,jp.thiran}@epfl.ch,

[2]Service Médico-Pédagogique, Psychiatry Department,
University of Geneva School of Medicine, CH-1211 Geneva, Switzerland
Email: {marie.schaer,stephan.eliez}@medecine.unige.ch

[3]Imagerie pédiatrique et fœtale, Hôpital Debrousse,
Université Claude Bernard Lyon I, Lyon, France
Email: laurent.guibaud@chu-lyon.fr

ABSTRACT

In this work we present a method for the image analysis of Magnetic Resonance Imaging (MRI) of fetuses. Our goal is to segment the brain surface from multiple volumes (axial, coronal and sagittal acquisitions) of a fetus. To this end we propose a two-step approach: first, a Finite Gaussian Mixture Model (FGMM) will segment the image into 3 classes: brain, non-brain and mixture voxels. Second, a Markov Random Field scheme will be applied to re-distribute mixture voxels into either brain or non-brain tissue. Our main contributions are an adapted energy computation and an *extended* neighborhood from multiple volumes in the MRF step. Preliminary results on four fetuses of different gestational ages will be shown.

1. INTRODUCTION

Development of the fetal brain surface which characterizes gyration is one of the major maturational processes of the human brain. The gyration, which was initially studied by neuropathologists [1, 2], can be followed on prenatal imaging as suggested first by Droulle using ultrasound [3, 4, 5] and shown more recently in fetal cerebral MRI atlases [6, 7]. Fetal MRI is now a well recognized tool for cerebral anatomy evaluation especially for analysis of the cortex. However, this analysis remains qualitative using the progressive identification of the primary and secondary gyri along the second and third trimesters of the pregnancy. A quantitative analysis of cortical surface can represent a new approach which can be used as a marker of the cerebral maturation and also for studying central nervous system (CNS) pathologies. However, this quantitative approach is a major challenge for two reasons: first, movement of the fetus inside the amniotic cavity requires very fast MRI sequences, hence resulting in a poor spatial resolution; second, due to the ongoing myelination and cortical maturation, the appearance of the developing brain differs from the easily segmented homogenous tissue types found in adults. To overcome the low resolution issue, Rousseau et al. [8] and Jiang et al. [9] built super-resolution images of the fetal brain from different acquisitions, but no segmentation method was proposed. To avoid motion artifacts, few studies use cerebral MRI obtained from premature neonates to quantitatively measure early brain development [10, 11, 12, 13]. However, this strategy does not allow the study of normal brain development over a large age range, since the most premature births are not likely to represent appropriate specimen for the study of normal development. In fact, so far few works have studied the brain segmentation of fetal MR images [14].

This work is a first attempt to automatic brain segmentation of MR brain images of fetus. We propose a Finite Gaussian Mixture Model (FGMM) and a Markov Random Field (MRF) scheme to perform brain surface segmentation. This combinations is very often used on adults brains [19] and has been successfully applied to premature neonates [10]. We modify the MRF energy to correct partial volume voxels and we present also an *extended* neighborhood. This article is organized as follows. The data set and the proposed segmentation method are described in Section 2. Segmentation results are discussed in Section 3. Finally, conclusions and future research are presented in Section 4.

2. METHOD

2.1 Data set

Prenatal MR imaging was performed with a 1-T system (GE Medical Systems, Milwaukee) using SSFSE sequences (TR 7000 ms, TE 180 ms, FOV 40 x 40 cm, slice thickness 5 mm, in plane spatial resolution 0.78 mm). Four fetal cerebral MR studies were retrospectively reviewed including exams of fetuses at 23, 27, 28.5, 32 weeks of gestation. Each study included volumes acquired in axial, sagittal and coronal views for a total of

This work is supported by the Center for Biomedical Imaging (CIBM) of the Geneva - Lausanne Universities and the EPFL, and the foundations Leenaards and Louis-Jeantet, and by the Swiss National Research Funds to Dr. Marie Schaer (323500-111165) as well as to Dr. Stephan Eliez (3200-063135, 3232-063134, and PP00B-102864).

15 planes for each volume. Acquisition times were about 1 minute for every image volume.

2.2 Pre-processing

Two pre-processing steps are needed before brain surface segmentation: inhomogeneity intensity correction and skull stripping. The inhomogeneity of the magnetic field creates an intensity variability in the MRI images. To correct this disturbance, a bias correction is applied [15, 16]. However, some intensity inhomogeneity mainly due to intra-tissue variability of developing brain will still remain. Finally, the skull stripping which isolates the intracranial cavity is completed by using a fast and robust active contour segmentation approach [17] and is then manually corrected.

2.3 Brain tissue classification

The fetal brain segmentation into brain (gray matter, GM, and white matter, WM, myelinated or not) and non-brain (mainly cerebrospinal fluid, CSF) tissues is performed in two steps. A Finite Gaussian Mixture Model (FGMM) is first adopted to classify each voxel according to their intensities. Thus, we aim at classifying the fetal brain into two classes: Brain and Non-brain tissue. To this purpose, 5 labels (L) are used: two for the *Brain* tissue class ($B = \{B_1, B_2\}$), two for the *Non-Brain* tissue class ($NB = \{NB_1, NB_2\}$) and a fifth one for *Transition* voxels (T). This last class represents uncertainty voxels between GM and CSF. These voxels will be re-classified later into the two classes (*Brain* and *Non-brain*) with the MRF scheme. The choice of using two classes for each tissue has been done empirically.

2.3.1 Finite Gaussian Mixture Model (FGMM)

Let us denote y_i the gray level (intensity) of a voxel within an image S, $i \in S = \{1, 2, ..., N\}$ to be classified, $x_i \in L$ the corresponding labels, and X, Y the random variables associated. Let us suppose that the random variables Y_i are identically and independently distributed, then probability density function of the intensity voxel is given by:

$$P(y|\theta) = \sum_{\forall x \in L} P(x) \cdot P(y|x) = \sum_{\forall x \in L} \omega_x \cdot f(y|\theta_x). \quad (1)$$

$P(x) = \omega_x$, also called *mixture parameters*, is the prior probability of the label class x (thus, the random variables X_i are also assumed independent of each other). $P(y|x)$ is the conditional probability density function of y given the tissue class x. Here a Gaussian distribution, $f(y|\theta_x)$, is assumed for each label and it is defined by the parameters $\theta_x = (\mu_x, \sigma_x)$, the mean and standard deviation respectively. Under the constraint $\sum_{\forall x \in L} \omega_x = 1$, the aim is to estimate the unknown parameters $\boldsymbol{\theta} = (\theta_x, \omega_x)$ that maximize the log-likelihood function

$$\hat{\boldsymbol{\theta}} = \arg\max_{\theta} P(y|\boldsymbol{\theta}). \quad (2)$$

One common solution to this optimization problem is the expectation-maximization (EM) algorithm [18, 19]. Initial parameters are needed to start EM optimization: μ_xs are manually selected from the image histogram, $\omega_x = 1/5$ for every label (the assumption that all classes are initially equiprobable is done), and σ_xs are arbitrarily set to 5. Note that the use of two labels for each tissue enables us to be more robust concerning the histogram variability across differently myelinated fetuses. Moreover, the two classes have an anatomical meaning within the Brain tissue class since each Gaussian models the white matter and the gray matter even if the distinction between the two are not clearly defined for fetal brains.

Finally, once the optimal parameters $\hat{\theta}$ have been found, classification is performed by choosing for each voxel the class that maximizes the posterior probability $P(x|y)$ (MAP estimation). In fact, thanks to Bayes theorem, this is simplified by finding the limits of $\omega_x P(y|x)$ on the image histogram (Fig. 1(a)) and thresholding the image with these results (Fig. 1(b)).

2.3.2 Markov Random Field Model (MRF)

At this point, we have for every fetus three label maps corresponding to the FGMM segmentations of the three acquisition volumes, namely L_a, L_c, L_s. The MRF [21] will now use spatial information to reclassify every voxel of the T label in the two tissues brain ($B = \{B_1, B_2\}$ and non-brain ($NB = \{NB_1, NB_2\}$). Moreover, the intracranial cavity voxels wrongly classified as brain by the FGMM, typically voxels not segmented by the skull-strip, will be corrected by our MRF scheme. To this end, no intensity information is taken into account within the MRF.

Practically, the set of label voxels $x = \{x_1, x_2, .., x_i, .., x_N\}$ is assumed to be a realization of a random field $X = \{X_1, X_2, .., X_N\}$. X is said to be a MRF on S with respect to a neighborhood system $\mathcal{N}$ if and only if Positivity ($P(X) > 0, \forall x \in \mathcal{X}$, where $\mathcal{X}$ represents the space of all possible configurations) and Markovianity conditions are satisfied [22]. Markovianity says that:

$$P(x_i|x_{S-\{i\}}) = P(x_i|x_{\mathcal{N}_i}), \quad (3)$$

where the sites in the image S are related with a neighborhood system $\mathcal{N} = \{\mathcal{N}_i, i \in S\}$, where $\mathcal{N}_i$ is the set of sites neighboring i, with $i \notin \mathcal{N}_i$, and $i \in \mathcal{N}_j \Leftrightarrow j \in \mathcal{N}_i$. Intuitively, Eq. 3 says that spatial relationships between a voxel and the rest of the image can be reduced to the spatial interactions within a local neighborhood. A second order neighborhood system is exploited here, that is, the eight voxels in the slice and the nine in the two adjoining slices form the 26 voxels of the neighborhood ($n = 26$) of the voxel i.

Thanks to the Hammersley-Clifford theorem, we can describe the random field by a Gibbs distribution:

$$P(x_i|x_{\mathcal{N}_i}) = \frac{e^{-U(x)}}{\sum_{x \in \mathcal{X}} e^{-U(x)}}, \quad (4)$$

where $U(x)$ is the *energy function*. The denominator of the above equation is theoretically well-defined but it may be intractable since the sum among all possible configurations is usually not known. Instead, the conditional probabilities $P(x|x_{\mathcal{N}_i})$ are normalized by forcing

$$\sum_{\forall x_i \in L} P(x_i|x_{\mathcal{N}_i}) = 1. \quad (5)$$

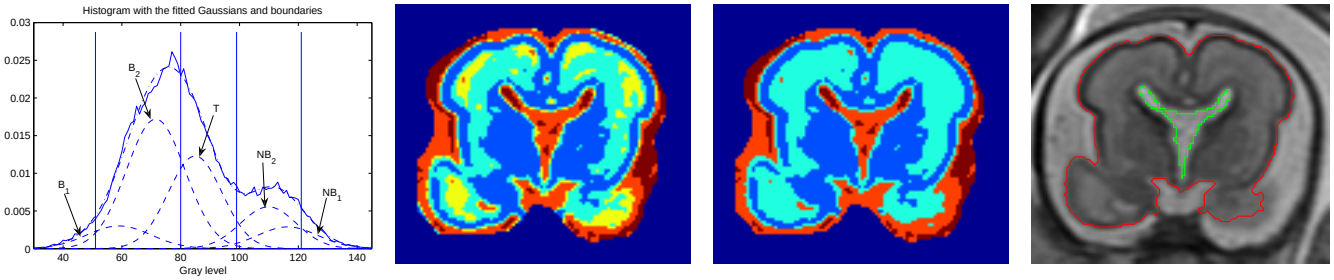

(a) Image histogram (solid line), fitted Gaussians (dotted line), and the sum of the Gaussians (dashed line).

(b) FGMM

(c) MRF

(d) Contours of the fetal brain.

Figure 1: Steps of the brain segmentation. The two tissues *Brain* (B) and *Non-brain* (NB) are represented by the labels: B_1, dark blue, B_2, light blue, NB_2, orange, and NB_1, red. *Transition* label is in yellow.

A new label map is found through Maximum a posteriori (MAP) of Eq. 3, that is equivalent to:

$$\hat{x} = \arg\min_{\forall x \in L}(U(x))). \tag{6}$$

This optimization problem is computationally infeasible but locally optimal solutions can be computed by iterative optimization techniques [22].

The energy function can be defined as follows:

$$U(x) = \sum_{\forall i \in S} \left(V_i(x_i) + \sum_{j \in \mathcal{N}_i} V_{ij}(x_i, x_j), \right), \tag{7}$$

where $V_i(x_i)$ is an external field that weights the relative importance of the different classes present in the image and V_{ij} models the interaction between neighbors [20]. Here, $V_i(x_i) = 0$ and

$$V_{ij}\,(x_i, x_j) = \frac{\delta_0(x_i, x_j)}{d(i,j)}, \tag{8}$$

which $\delta_0(x_i, x_j) = -1$ if $x_i = x_j$ and 0 otherwise, encourages voxels to be classified like the majority of its neighbors, weighted by the Euclidean distance between neighbors $d(i,j)$.

Here, δ_1 and δ_2 will be used instead. We define δ_1 to correct peripheral errors by associating voxels B near a voxel outside intracranial cavity (0 value) as NB:

$$\delta_1(x_i, x_j) = \begin{cases} -3, & \text{if } x_j = 0 \text{ and } x_i = NB \\ 0, & \text{otherwise.} \end{cases} \tag{9}$$

This simply means that brain tissue cannot directly touch the skull. This model is used once to correct peripheral voxel incorrectly classified. A second model to distribute voxels classified as transition label T is then used:

$$\delta_2(x_i, x_j) = \begin{cases} -3, & \text{if } x_j = 0 \text{ and } x_i = NB \\ -3, & \text{if } x_j = NB_1 \text{ and } x_i = NB \\ -2, & \text{if } x_j = NB_2 \text{ and } x_i = NB_2 \\ -1, & \text{if } x_j = T \text{ and } x_i = T \\ -2, & \text{if } x_j = B_2 \text{ and } x_i = B_2 \\ -3, & \text{if } x_j = B_1 \text{ and } x_i = B \\ 0, & \text{otherwise.} \end{cases} \tag{10}$$

This model classifies the voxels like the majority of its neighbors, but in order to suppress the T class, less weight is given to the T neighbors. Since there is more certainty that NB_1 and B_1 are part of tissue NB or B then NB_2 and B_2, they have a bigger influence.

Figure 1 illustrates the process of the brain segmentation using FGMM and MRF, and merging the labels B_1, B_2 and NB_1, NB_2 that allow us to obtain the contours of the brain of a 27 weeks old fetus.

2.4 Surface reconstruction

In this section we construct the 3D brain surface that combines the contours obtained from L_s, L_c and L_a. To this end, probability maps are constructed by:

$$P(i) = \begin{cases} \frac{1}{2+2d^2}, & \text{if } i \text{ inside C} \\ 1 - \frac{1}{2+2d^2}, & \text{otherwise,} \end{cases} \tag{11}$$

where d is the Euclidean distance to the brain contour C and i is a voxel location. Probability maps are used instead of Label maps, which allows to combine them by linear interpolation. To combine the 3 probability volumes, the three image volumes must be aligned first. Thus, inter-volume registration is needed to compensate for different position of the fetus across axial, coronal and sagittal acquisitions. To this end, by maximization of mutual information, 3D rigid registration (3 rotation and 3 translations) is computed on the gray level images (implemented in ITK [15]). Then, the rigid transformation is applied using tri-linear interpolation on the probability maps. By applying a threshold to the resulting distance map at 0.5 we obtain the brain surface.

2.5 Extended MRF Neighborhood

Instead of combining the 3 acquisitions in a final step only, we propose to profit from all 3 acquisition volumes within the MRF framework. We add up to 9 neighbors per volume, for instance from L_a and L_c, to the 26 neighbors of L_s. To implement such extended neighborhood, rigid transformation is applied to labeled images. Once a point to point correspondence is obtained, the corresponding voxel within the complementary volumes and its 8 neighbors are considered for the MRF energy computation. It might occur that no information is contained in some of the extended neighbors. The scheme of extended neighborhood is represented in Fig. 2.

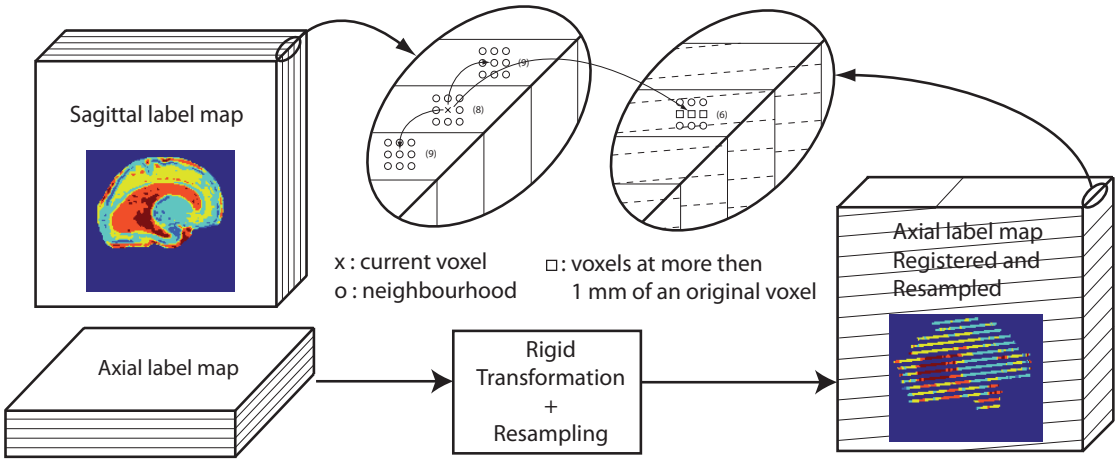

Figure 2: Scheme of the proposed extended neighborhood.

3. RESULTS

Our segmentation method has successfully been tested on four fetuses of different age: 23, 27, 28.5 and 32 weeks old. The results of the segmentation are presented in Figure 3. Unfortunately, at this stage, only visual assessment can be done due to the lack of manual segmentations or other ground truth. The construction of a 3D volume which represents the brain of the fetus is shown in Figure 5. We can see the difference of gyration between the two volumes: the youngest fetus is very smooth whereas the older one presents more sulci and gyri. In Figure 4, we compare the contour extracted from one single acquisition (L_s) and the one from the fusion of the 3 acquisitions. Despite better depth resolution obtained, in plane segmentation presents less precision in sulci.

Figure 6 compares the results of the segmentation with and without the extended neighborhood. As expected, the extended neighborhood improves the MRF within a single volume only in the areas where reliable information can be obtained, when a perfect point-to-point correspondence exists across the 3 image acquisitions (see for instance the ventricle contour in extended MRF in Fig. 6(b)). Unfortunately, other regions (see for instance frontal lobe in Fig. 6(b)) are less accurately segmented. Computation time was about 4 min for the FGMM and MRF scheme and 10 min for the extended Neighborhood with an Intel Core 2 Duo T7300 (2 GHz).

3.1 Discussion

Our FGMM and MRF scheme performs well but limited accuracy has been obtained in gyri and sulci. This is mainly due to very large slice thickness and fetal motion. Even if rigid registration is applied to correct fetal movement between acquisition volumes, intra-volume fetus motion still remains; this is the case in Figures 4 and 6. As proposed by [10], one possible correction of this motion is to perform a 2D-3D registration: using as reference image a high resolution (HR) volume which combines the three low resolution (LR) acquisitions in order to register each 2D slice of the LR images.

Further development must also be done for the sur-

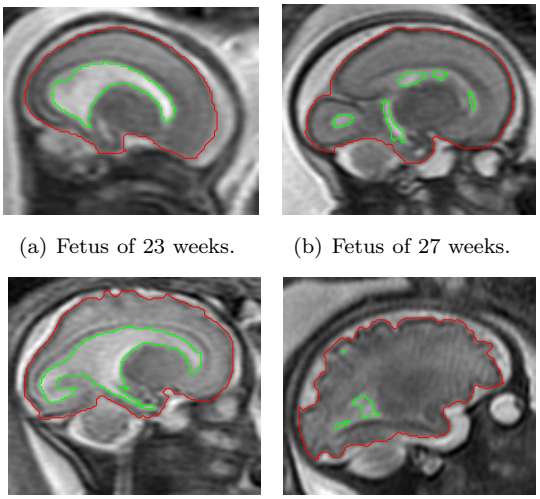

(a) Fetus of 23 weeks. (b) Fetus of 27 weeks.

(c) Fetus of 28.5 weeks. (d) Fetus of 32 weeks.

Figure 3: Results of the brain segmentation.

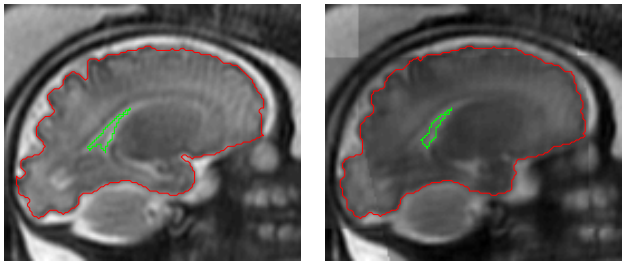

(a) Contours from L_s (b) Contours from L_s+L_a+L_c

Figure 4: Comparison between a single acquisition and the combination of 3 acquisition volumes.

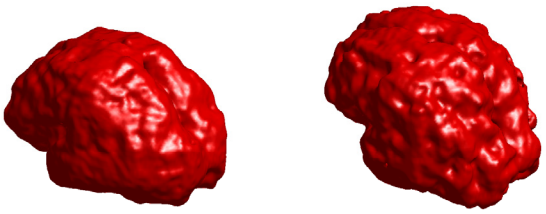

(a) Fetus of 27 weeks. (b) Fetus of 32 weeks.

Figure 5: 3D volume which represents the brain of the fetus.

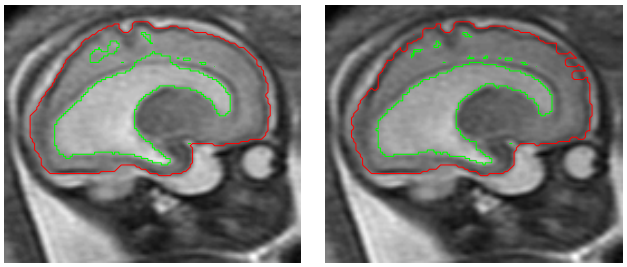

(a) MRF segmentation (b) Extended neighborhood

Figure 6: Comparison of MRF segmentation with an extended neighborhood.

face reconstruction. In this paper, reconstruction has only been applied for visualization. However, more evolved methods should be applied for cortical folding reconstruction and quantitative measures such as parametric deformable models [23] or geometric deformable models [24].

4. CONCLUSION

In this work, a brain segmentation method of MRI of the fetus has been proposed. To our knowledge, this is the first attempt to perform automatic segmentation of such image data. We proposed a FGMM and MRF scheme to solve the tissue segmentation problem. Our main contribution is an adapted energy computation and an extended neighborhood in the MRF step. Four fetuses of different gestational age have been successfully segmented and 3D brain surfaces have been created. Visual validation has been carried out showing some limitations of our approach mainly due to low depth resolution ($5mm$) and intra-volume fetal motion. Thus, further work will mainly focus on compensating for such motion artifacts and increasing the accuracy of the brain contours. Moreover, quantitative validation work will be drive on high resolution MRI acquired on premature neonates.

REFERENCES

[1] J.C. Larroche, "Development of the nervous system in early life, II: the development of the central nervous system during intrauterine life." In: Falkner F, ed. Human Development. Philadelphia, Pa: WB Saunders; pp. 257276. 1966.

[2] Feess-Higgins et al, "Le dveloppement du cerveau ftal humain. Atlas anatomique", INSERM. CNRS, Masson, Paris, pp. 1-200 , 1987.

[3] P. Droulle et al., "Maturation of the fetal brain. Echoanatomy: normal development, limits and value of pathology". J Gynecol Obstet Biol Reprod, vol. 13, no. 3, pp. 228-36, 1984.

[4] C. Bernard et al., "Echographic aspects of cerebral sulci in the ante- and perinatal period.", J Radiol. vol. 69, pp. 521-32, 1988.

[5] E. Quarello et al., "Assessment of the sylvian fissure development between 22 to 32 weeks of gestation", submitted to Ultrasound Obstet Gynecol, 2008.

[6] C. Garel, "MRI of fetal brain. Normal development and cerebral pathologies.", Heidelberg, Springer-Verlag, 2004.

[7] C. Adamsbaum et al., "Atlas dIRM du cerveau fetal," 1er ed Paris, Masson, 2004.

[8] F. Rousseau et al., "Registration-Based Approach for Reconstruction of High-Resolution In Utero Fetal MR Brain images," IEEE Transactions on Medical Imaging, Academic radiology, vol. 13, no. 9, pp. 1072–1081, 2006.

[9] S. Jiang et al., "MRI of Moving Subjects Using Multislice Snapshot Images With Volume Reconstruction (SVR): Application to Fetal, Neonatal, and Adult Brain Studies,"IEEE Transactions on Medical Imaging, vol. 26, no. 7, pp. 967–980, July 2007.

[10] H. Xue et al., "Automatic segmentation and reconstruction of the cortex from neonatal mri," NeuroImage, vol. 38, no. 3, pp. 461477, novembre 2007.

[11] J. Dubois et al. "Mapping the early cortical folding process in the preterm newborn brain", Cerebral Cortex, vol. 18, no.6, pp. 1444-1454, October 2007.

[12] H. Merisaari et al., "Quantification of the premature infant brain volume from MR images using watershed transform and bayesian segmentation,"vol. 3, no. 12, pp. 11171121, 2007.

[13] M. Prastawa et al., "Automatic segmentation of MR images of the developing newborn brain," Medical Image Computing and Computer-Assisted Intervention - MICCAI 2004, vol. 9, no. 5, pp. 457466, Octobre 2005.

[14] I. Claude et al., "Fetal Brain MRI: Segmentation and Biometric Analysis of the Posterior Fossa," IEEE Transactions on Biomedical Engineering, vol. 51, no. 4, pp. 617–626, Avril 2004.

[15] ITK, "Insight Registration and Segmentation Toolkit", www.itk.org.

[16] M. Styner, et al., "Parametric estimate of intensity inhomogeneities applied to MRI", IEEE Trans. on Medical Imaging, vol. 19, no. 3, pp. 153-165, 2000.

[17] X. Bresson et al.,"Fast Global Minimization of the Active Contour/Snake Model," Journal of Mathematical Imaging and Vision (JMIV), vol. 28, no. 2, pp. 151–167, 2007.

[18] R. O. Duda et P. E. Hart, "Pattern Classification and Scene Analysis," S. R. Institute, Ed. New York: Wiley, 1973.

[19] M. Bach Cuadra et al., "Comparison and Validation of Tissue Modelization and Statistical Classification Methods in T1-weighted MR Brain Images," IEEE Transactions on Medical Imaging, vol. 24, no. 12, pp. 15481565, 2005

[20] N. Peyrard, "Approximations de type champ moyen des modèles de champ de Markov pour la segmentation de donnes spatiales," Ph.D. Dissertation, University J. Fourier, Grenoble, France, Oct. 2001.

[21] J. Zhang, "The mean field theory in EM procedures for Markov random fields," IEEE Trans. Signal Process., vol. 40, no. 10, pp. 25702583, Oct. 1992.

[22] Stan Z. Li, "Markov Random Field Modeling in Image Analysis", Computer Science Workbench, Springer 2001.

[23] A.M. Dale et al., "Cortical surface-based analysis I: segmentation and surface reconstruction," Neuroimage, vol. 9, pp. 179–194, 1999.

[24] X. Han et al., "CRUISE: cortical reconstruction using implicit surface evolution," Neuroimage, vol. 23, pp. 997–1012, 2004.